ChemElectroChem

Chemistry Europe
European Chemical Societies Publishing

Reprint

WILEY-VCH

Special Collection

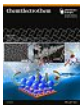

An Electrochemically Synthesized Nanoporous Copper Microsensor for Highly Sensitive and Selective Determination of Glyphosate

Matias Regiart,[a] Abhishek Kumar,*[a, d] Josué M. Gonçalves,[b] Gilberto J. Silva Junior,[a] Jorge César Masini,[c] Lúcio Angnes,[b] and Mauro Bertotti*[a]

A nanoporous copper (NPC) film was electrodeposited on a copper microelectrode, and the generated platform was investigated for electrochemical sensing of glyphosate (Glyp). The as-deposited NPC film was highly pure and crystalline according to results of energy dispersive spectroscopy and X-ray diffraction experiments, respectively. Scanning electron microscopy images confirm the NPC films possess a highly porous morphology containing dendrite fractals, and the electrodeposition parameters, particularly potential (E_d) and time (t_d), exert a remarkable influence on the structure of the films. Such changes in the NPC morphology with E_d and t_d were also correlated with the electrochemical behavior investigated by cyclic voltammetry. In the presence of Glyp, the anodic oxidation is facilitated because copper ions diffuse easily through the pores of the NPC film and form a complex with the analyte at the electrode interface. On the other hand, as the amount of copper oxides decreases due to the formation of soluble Cu(II) complex with Glyp, less current is obtained during the reverse scan, allowing a relationship between the decrease in the cathodic current and the Glyp concentration to be established. The optimized NPC-modified Cu microelectrode showed very high sensitivity (14 nA nmol^{-1} L), low detection limit (4 nmol L^{-1}), excellent reproducibility, and selective response for Glyp. The applicability of the sensor was demonstrated by detecting Glyp in river water samples.

1. Introduction

N-(phosphonomethyl)glycine, also known as glyphosate (Glyp), is currently the most widely used herbicide in controlling weeds in agricultural activities. Glyphosate is a non-selective, post-emergent, and systemic herbicide that is absorbed by the foliage of plants and translocated throughout within it. Its phytotoxic activity is based on the inhibition of a specific plant enzyme (enolpyruvyl shikimate-3-phosphate synthase) during the flavonoids synthesis, which is fundamental to the formation of crucial aromatic amino acids necessary for the growth of plants.[1] However, the indiscriminate and large scale use of Glyp has resulted in its accumulation in the soil, which adversely affects soil microbial communities and nutrients.[2] It can also enter into the biological food chain, affecting the lives of humans and animals.[3,4] Moreover, because of the highly polar nature of the molecule, it is highly soluble in water and can contaminate water resources and thus poses a grave concern to the aquatic life.[5] A recent report of the World Health Organization has classified this herbicide as potentially carcinogenic to humans if exposed for a long term,[6] and this is also supported by several case studies.[7,8] Based on the health hazards and environmental risks, environmental protection and health care agencies have set the maximum acceptable level of the compound in drinking water as 0.70 mg L^{-1} in the USA[9] and only 0.1 μg L^{-1} in the EU.[10] Therefore, it is essential to continuously monitor Glyp levels in different water resources in order to implement those guidelines strictly and to mitigate health risks.

Different analytical methods previously employed to determine Glyp were comprehensively reviewed in the literature,[11–13] and most of them are based on chromatographic techniques.[14–17] These techniques are highly sensitive and can detect Glyp well below the defined guidelines in the targeted samples. However, such methods are extensively complex because liquid chromatography coupled with UV or fluorimetric detectors requires a chromophore. Hence, the Glyp molecule must be derivatized, and this often involves lengthy chemical procedures. Besides chromatographic methods, analytical ap-

[a] Dr. M. Regiart, Dr. A. Kumar, G. J. Silva Junior, Dr. M. Bertotti
Laboratório de Sensores Eletroquímicos e Métodos Eletroanalíticos
Department of Fundamental Chemistry, Institute of Chemistry
University of São Paulo, Av. Professor Lineu Prestes
748, 05513-970, São Paulo – SP, Brazil
E-mail: Abhishek.Kumar@u-bourgogne.fr
mbertott@iq.usp.br
[b] Dr. J. M. Gonçalves, Dr. L. Angnes
Laboratório de Automação e Instrumentação Analítica
Department of Fundamental Chemistry, Institute of Chemistry
University of São Paulo, Av. Professor Lineu Prestes
748, 05513-970, São Paulo – SP, Brazil
[c] Dr. J. C. Masini
Laboratório de Química Analítica Ambiental
Department of Fundamental Chemistry, Institute of Chemistry
University of São Paulo, Av. Professor Lineu Prestes
748, 05513-970, São Paulo – SP, Brazil
[d] Dr. A. Kumar
Current address:
Institut de Chimie Moléculaire de l'Université de Bourgogne
(ICMUB), UMR CNRS 6302, Université Bourgogne Franche-Comté, 9 avenue
Alain Savary, 21078 Dijon cedex, France

Supporting information for this article is available on the WWW under https://doi.org/10.1002/celc.202000064

An invited contribution to a Special Collection on Electrochemical Sensing

© 2020 Wiley-VCH Verlag GmbH & Co. KGaA, Weinheim

proaches based on fluorescence[18] and electrophoresis[19] have also been employed for sensitive and selective detection of Glyp in river water and soil samples. Nevertheless, these methods are highly expensive, require lengthy analysis time, and depend on bulky instrumentation; thus, they are unsuitable for field monitoring.

Electrochemical sensors are a suitable alternative possessing the advantages of high sensitivity, selectivity, real-time monitoring, low cost, and miniaturization. However, as Glyp is not an electrochemically active compound within the accessible potential range, approaches based on indirect electrochemical sensing have been developed using different electrodes such as gold, platinum, nickel, copper, and cobalt.[20–23] In these previous studies, non-noble metal electrodes, especially copper, were a preferred choice because noble metals electrodes suffer from surface fouling from strong irreversible adsorption of Glyp amino and carboxylic moieties. Copper-based organometallic compounds like copper phthalocyanine composited with carbon nanotubes were also used for direct voltammetric determination of Glyp,[24] and the developed sensor showed very high sensitivity and detection limit in the nmol L^{-1} range, which is below the mandated guidelines. In recent years, different types of nanomaterials like layered double hydroxides,[25] electrogenerated copper nanoparticles,[26] copper-based metal-organic framework,[27] and copper nanowires[28] have been used to detect Glyp, and they have exhibited very high sensitivity and selectivity towards such analyte. Besides nanomaterials based on copper, cross-linked imprinted polymer modified carbon[29] and anti-glyphosate antibody-modified magnetic beads based screen-printed electrodes[30] have been also used in the development of highly sensitive and selective electroanalytical platforms for Glyp determination. However, such electrochemical detection methods involve a complex and long electrode processing step, either to synthesize polymers or to immobilize enzymes.

Copper electrodes have been used to detect Glyp because when polarized at potentials close to 0.0 V, a film of hydrated copper oxides is generated on the surface, and the solubility of such film increases when compounds that form stable complexes with Cu(II) are present in the solution. Hence, in solutions containing Glyp, the amount of copper oxides decreases, and less current is obtained during the reverse scan towards more negative potentials. Then, a relationship between the reduction in the cathodic current and the concentration of Glyp in the solution can be established.[20–22] Taking into account the complexation tendency of copper cations with Glyp, the use of nanoporous copper (NPC) with very high surface area can be an ideal sensing material for the development of an ultra-high sensitivity method for this pesticide detection.

Such nanoporous materials have drawn tremendous attention in recent years in the field of electrochemical sensors, and they are characterized by a bicontinuous network of interconnected nanometric copper struts and multiple sized pores, forming a 3-dimensional architecture like a metallic foam. NPC materials have been mainly synthesized by electrochemical methods such as dealloying of a copper-containing alloy[31,32] and template-assisted electrodeposition from a copper precursor solution.[33,34] The main advantage of such electrosynthesis approaches is a fine-tuning of the nanoporous features like struts and pores by modulating the electrodeposition experimental parameters to produce a porous film desired for a particular application. NPC materials were widely investigated in the field of electrochemical sensors to detect glucose,[35] nitrate,[36] nitrite,[37] oxygen,[38] among others. Interestingly, NPC materials have not been appropriately investigated to develop a sensor for Glyp, and minimal information is available in the previous literature.

Accordingly, herein we present a facile synthesis of an NPC modified copper microelectrode by Dynamic Hydrogen Bubble Template (DHBT) method[39] and the application of such a platform for voltammetric determination of Glyp in water samples. Our strategy is based on optimizing the electrodeposition parameters, particularly deposition potential (E_d) and deposition time (t_d), in the electrosynthesis of NPC to achieve a highly porous film (with large surface area) for the optimum sensing of Glyp. The chemical purity and crystalline structure of the obtained NPC films were ascertained by Energy Dispersive X-ray Spectroscopy (EDS) and X-Ray Diffraction (XRD), respectively. The morphology of different NPC films was characterized by Scanning Electron Microscopy (SEM). The available information on the film property and structure was correlated with the applied electrodeposition parameters and further with the NPC electrode electrochemical response in the presence of Glyp. The electrochemical behavior of the optimized NPC modified copper microelectrode was extensively characterized by cyclic voltammetry (CV) to assess different electroanalytical parameters for Glyp determination. Finally, any possible interference from other species that usually coexist with Glyp in real samples and the applicability of the sensor in detecting Glyp in river water samples were also evaluated.

Experimental Section

Reagents and Solutions

All the reagents employed were of analytical grade, and they were used without further purification. Glyphosate, simazine, propazine, atrazine, aminomethylphosphonic acid (AMPA), and copper sulfate pentahydrate ($CuSO_4 \cdot 5H_2O$) were purchased from Sigma Aldrich (St. Louis, USA). Phosphate Buffer Saline (PBS) tablets were obtained from Merck (Darmstadt, Germany) and were adequately dissolved in 200 mL of water to prepare 0.1 mol L^{-1} PBS buffer of pH 7.0. Milli-Q ultrapure water (resistivity ~ 18 MΩ cm) was used to prepare all aqueous solutions.

Electrochemical Setup

All electrochemical measurements were performed on an Autolab PGSTAT128N potentiostat interfaced with NOVA 1.11 software. The experiments were carried out in a conventional three-electrode cell using a copper disc microelectrode as the working electrode and a Ag/AgCl (saturated KCl) and a platinum wire as reference and counter electrodes respectively. The copper disc microelectrode was fabricated by sealing a copper microfiber (Puratronic® – Alfa Aesar) with a nominal radius of 12.5 μm directly to a Pasteur pipette using Araldite epoxy resin, according to a standard procedure

© 2020 Wiley-VCH Verlag GmbH & Co. KGaA, Weinheim

previously described.[40] The microelectrode was further polished with sandpaper and alumina slurry (0.05 μm), followed by sonication for 3 minutes in distilled water.

Electrodeposition of NPC

All NPC electrodepositions were carried out through the potentiostatic DHBT method by applying a fixed potential for a given time in a 0.5 mol L^{-1} H_2SO_4 stirred solution containing 5 mmol L^{-1} $CuSO_4$, at open atmosphere and room temperature. Two sets of NPC films were electrodeposited: a) at applied potentials of −1 V, −2 V, −3 V, and −4 V for a fixed time of 150 s and (b) at applied potential of −3 V for different times: 25 s, 50 s, 100 s, 150 s, and 200 s. Electrodeposited NPC films were subsequently washed with water and dried at room temperature. The stirring rate was maintained constant to obtain reproducible results at each experimental condition, and the working electrode was always placed at the same distance from the rotating magnetic bead during the electrodeposition step.

Structural and Morphological Characterization

NPC surface morphology was investigated using a JEOL JSM-FEG 7401F SEM equipment at an accelerating voltage of 2 kV at different magnifications. In-plane and cross-section SEM images were recorded, which were further analyzed with ImageJ software. EDS spectra of the NPC films were also recorded at the same equipment to get information about the elemental composition.

NPC crystalline structure was evaluated by XRD performed in a tabletop Bruker D2 Phaser X-ray diffractometer equipped with a Cu Kα source (λ = 1.5418 Å) in the 2θ window of 40 to 80°, using a scan step of 0.05°.

Electrochemical Experiments

NPC modified Cu microelectrodes were characterized by CV recorded in 0.1 mol L^{-1} PBS buffer (pH 7.0) in a potential range from −0.5 V to 0.5 V at 25 or 50 mV s^{-1} scan rate. CVs were also recorded in the presence of Glyp varying the concentrations in the range from 30 nmol L^{-1} to 20 μmol L^{-1}. Interference studies were carried out by recording CVs in a 45 nmol L^{-1} Glyp solution in the presence of simazine, propazine, atrazine, AMPA, Na^+, K^+, Ni^{2+}, Ca^{2+} and Mg^{2+} at 10-fold higher concentration than that of the target analyte.

For the determination of Glyp in river water, the sample was taken in a pre-cleaned amber glass bottle (1000 mL), which was filled completely such that there was no air space in the bottle. The sample was then immediately placed in a cooler filled with ice and transferred to the laboratory for refrigerated storage at 4 °C until analysis, which was done within one week after collection in all instances. The sample was filtered through a 0.45 μm pore size Millipore mixed cellulose ester membrane filters, and the pH was adjusted to 7.0. The sample was then further diluted with PBS buffer. Finally, any possible presence of Glyp was assessed by standard addition method, in which the test sample was spiked with a standard Glyp solution.

2. Results and Discussion

2.1. Structure, Chemical Purity and Morphology of NPC

Since the electrodeposition of NPC was performed using a $CuSO_4$ precursor solution, sulfate remains a potential contaminant as it is prone to get adsorbed or trapped in the growing NPC film.[41] Therefore, to ascertain the chemical purity of the deposited NPC films, EDS spectra were recorded. Figure 1a shows the obtained spectrum, which exhibits a characteristic intense L_α band at 0.93 keV and a weaker K_α band at 8.04 keV associated with x-ray emissions from L and K shells of copper, respectively, thus confirming the growth of a pure copper film during the electrodeposition step. Moreover, any possible contamination from sulfate was also ruled out.

NPC crystallites microstructure and their orientations were assessed by XRD performed on the as-prepared NPC films at room temperature. Background corrected diffraction pattern of NPC electrodeposited at $E_d = -3$ V for 150 s is shown in Figure 1b, where three sharp diffraction peaks can be noticed at 43.4°, 50.5°, and 74.2° corresponding to (111), (200), and (220) facets, respectively, of an fcc lattice of copper [JCPDS 04-0836].[42] Hence, the preparation of NPC produced highly pure and polycrystalline copper films.

The surface morphology of the as-deposited NPC films on the copper microelectrode was examined by SEM imaging in which emphasis was given to understand the changes in the NPC morphology induced by varying the electrodeposition parameters (E_d and t_d). Figure 2 shows the SEM micrographs of NPCs electrodeposited in a range of E_d from −1 V to −4 V and for two different t_d values (50 s and 150 s). The image of the bare copper substrate is given in Figure 2i, and the surface

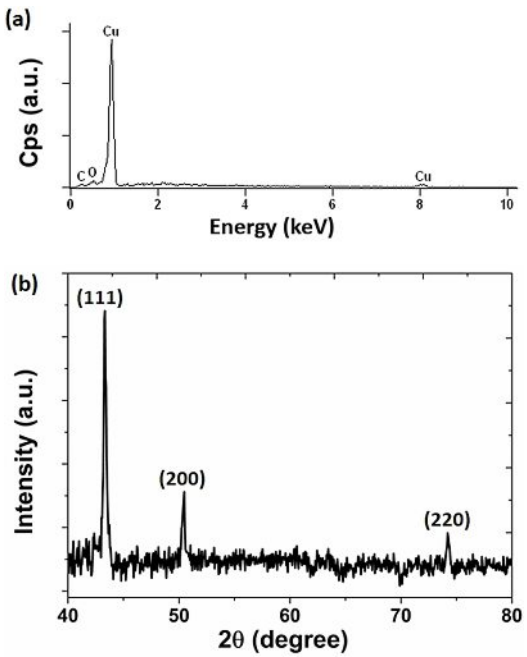

Figure 1. EDS spectrum (a) and XRD pattern (b) of NPC deposited at $E_d = -3$ V and $t_d = 150$ s on a copper microelectrode.

© 2020 Wiley-VCH Verlag GmbH & Co. KGaA, Weinheim

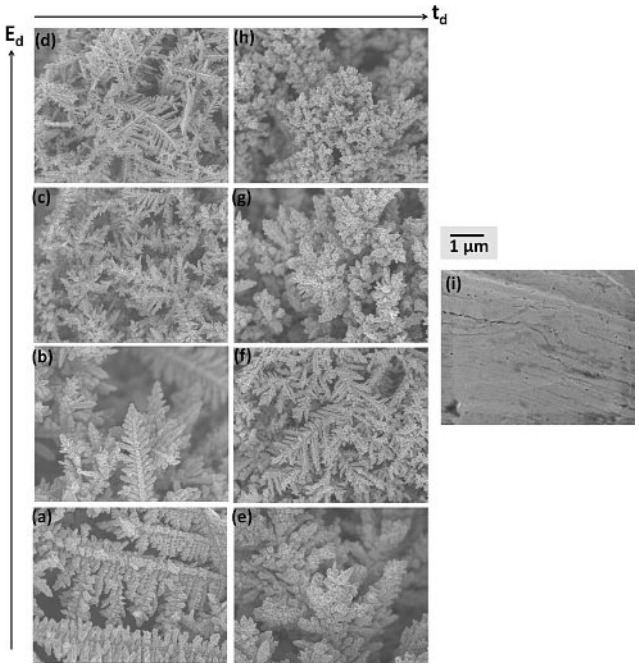

Figure 2. SEM images of NPC electrodeposited at −1 V for 50 s (a), −2 V for 50 s (b), −3 V for 50 s (c), −4 V for 50 s (d), −1 V for 150 s (e), −2 V for 150 s (f), −3 V for 150 s (g), −4 V for 150 s (h) and uncoated substrate (i).

appears to be highly smooth. The morphology of NPCs is characterized by micrometers long and highly branched copper fractals whose dimension, porosity, and size change as a function of E_d and t_d. At less negative potential value (E_d = −1 V), the fractals correspond to under-grown but very long dendrites, and this may be a consequence of the limited number of nucleation centers available on the copper substrate. This is in agreement with a growth mechanism following a combination of ballistic[43] and diffusion-limited aggregation[44] models, as also reported previously in our work on nanoporous gold films.[45] As E_d becomes more negative, the dendrites growth is more uniform, and their size becomes smaller and increasingly 2-dimensional, evidenced by a 2-D and homogeneously grown smaller dendrite at E_d = −4 V. Such transformations are attributed to the activation of nucleation centers on the copper substrate at more negative potentials, which were dormant at less negative E_d.

The influence of increasing t_d is also clearly evident on the NPC morphology as dendrites get smaller and highly branched, extending into 3-dimension, and the surface becomes more porous. Such changes can be mainly attributed to two factors: *i.* each depositing copper crystallite behaves like a new nucleation center for the incoming copper atoms, resulting in a considerable enhancement in the number of nucleation centers and *ii.* the diffusion regime changes from planer to spherical as the surface becomes rougher.[46] The shortening of the dendrites size and the enhancement in the branching have a profound implication on both surface area and porosity of the NPC films, which can contribute to improving the electrochemical sensing performance.

The high surface area and porosity of the NPC films were further illustrated by a cross-section SEM image, as shown in Figure 3. Highly branched and porous clusters of dendrites extending up to 30 μm in height can be noticed. A microporous honeycomb morphology with micropores in a range of 5–15 μm can be observed at a less magnified SEM image (Figure S1). In fact, such honeycomb morphology is a typical feature of DHBT electrodeposited films.[47]

2.2. Electrochemistry of the NPC Cu Microelectrode

2.2.1. The Influence of Glyp on the Electrochemical Behavior of the NPC Cu Microelectrode

Although Glyp is electrochemically inactive, this compound influences the electrochemical behavior of NPC materials through a chemical reaction with Cu(II) ions. Accordingly, changes in the NPC electrochemistry can be used as a strategy for indirect electrochemical sensing of Glyp. CVs of an NPC modified Cu microelectrode in a potential range from −0.5 V to 0.5 V in 0.1 mol L^{-1} PBS in the absence and presence of 60 nmol L^{-1} Glyp are shown in Figure 4. A broad anodic peak at 0.02 V, associated with the oxidation of copper into Cu^{2+}, and a

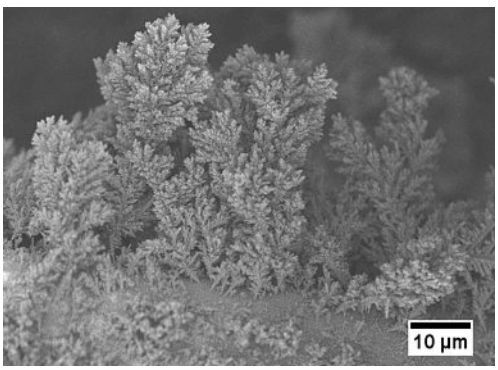

Figure 3. Cross-section view of the electrodeposited NPC film on a copper substrate (E_d = −3 V, t_d = 150 s).

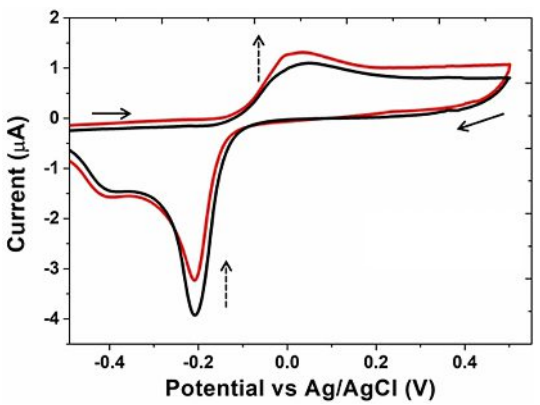

Figure 4. Voltammograms recorded with an NPC-modified Cu microelectrode (E_d = −3 V and t_d = 150 s) in 0.1 mol L^{-1} PBS (in black) and 0.1 mol L^{-1} PBS + 60 nmol L^{-1} Glyp (in red) at a scan rate of 25 mV s^{-1}.

© 2020 Wiley-VCH Verlag GmbH & Co. KGaA, Weinheim

sharp cathodic peak at −0.20 V, corresponding to the regeneration of copper from copper oxides and Cu^{2+} formed in the forward scan, are clearly seen.

The high permeability of the oxide layer formed in phosphate buffer makes possible the complexation of Cu(II) ions present in the porous outer layer with Glyp. Hence, an enhancement in the copper oxidation current is noticed in the presence of Glyp, promoting the electrochemical dissolution of copper.[48,49] In fact, the Glyp molecule contains amino, carboxylic, and phosphonate moieties, which can form a stable chelate with Cu^{2+}. On the other hand, a decrease in the cathodic current is observed as a consequence of the loss of copper oxides during the forward scan in the presence of Glyp. Taking into account that Cu(II) ions formed during the Cu anodic oxidation diffuse through the oxide layers and interact with Glyp, the film porosity may influence the rate of the electrode process.

A comparative study was performed with a bare Cu microelectrode to confirm the advantages of modifying the electrode surface. Accordingly, Figure 5 shows CVs recorded in 0.1 mol L^{-1} PBS in the absence and presence of 3 μmol L^{-1} Glyp. As expected, a reduction in the cathodic current is observed upon the addition of Glyp, but this is only noticed when the analyte concentration is in the μmol L^{-1} range. Hence, an NPC material with a high surface area would be advantageous for the enhancement of the sensor response, justifying studies regarding the optimization of the electrodeposition parameters E_d and t_d.

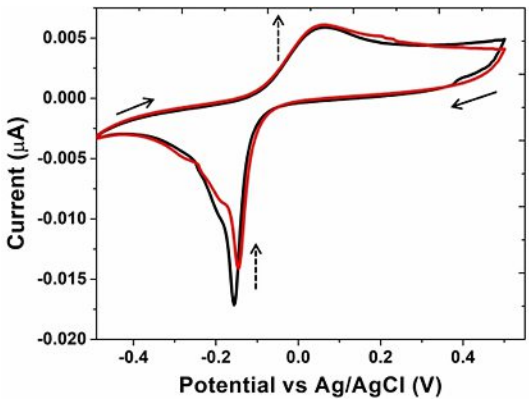

Figure 5. Voltammograms recorded with a bare Cu microelectrode in 0.1 mol L^{-1} PBS in the absence (black) and presence (red) of 3 μmol L^{-1} Glyp. Scan rate: 25 mV s^{-1}.

2.2.2. Optimization of E_d and t_d

CVs of NPC Cu microelectrodes prepared at different E_d and for varying t_d were recorded to obtain the NPC film most suitable for the development of a Glyp sensor. Figure 6a shows the results of such a comparative study carried out in 0.1 mol L^{-1} PBS in a potential range of −0.5 V to 0.5 V. The influence of E_d on the anodic and cathodic processes associated with corrosion and regeneration of copper at the electrode/electrolyte interface is evident. Notably, the oxidation current resulting from copper ion formation increases at more negative values, especially at $E_d = -4$ V, a condition that provides a larger pool of reactant for Glyp complexation. Such an enhancement in the copper corrosion current can be correlated with the increase in surface area and porosity of NPC as E_d becomes more negative, which is also evident from the SEM image shown in Figure 2h. However, because the voltammetric response regarding NPC modified Cu microelectrodes prepared at $E_d = -4$ V was not reproducible, subsequent experiments were performed with Cu microelectrodes modified at $E_d = -3$ V. It must also be highlighted that copper anodic oxidation current increases more than 300-fold for the NPC prepared at $E_d = -3$ V for 150 s in comparison to that for the bare Cu microelectrode (CV in the inset of Figure 6a).

The NPC films electrodeposited at −3 V were also optimized for different t_d (in a range of 25 to 200 s) under similar electrochemical experimental conditions, and a comparison of voltammograms is shown in Figure 6b. The increase in oxidation and reduction peaks with increasing t_d is noticeable, and this is a consequence of the shortening of the copper dendrites as visualized in the SEM images, thereby enhancing

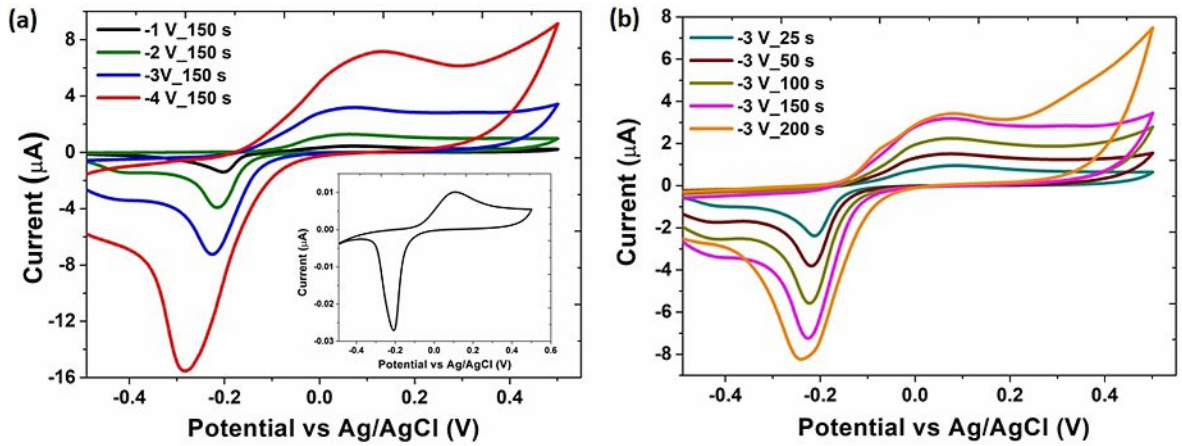

Figure 6. Voltammograms of NPC Cu microelectrodes recorded in a 0.1 mol L^{-1} PBS + 60 nmol L^{-1} Glyp solution: $E_d = -1$ V, −2 V, −3 V and −4 V for 150 s (a) and $E_d = -3$ V for 25 s, 50 s, 100 s, 150 s and 200 s (b). The CV of the bare Cu microelectrode is shown in the inset of (a). (scan rate: 50 mV s^{-1}).

© 2020 Wiley-VCH Verlag GmbH & Co. KGaA, Weinheim

the porosity and the surface area of NPC. Higher copper corrosion current ensures a massive reservoir of cuprous ions to be available for complexation with Glyp. However, saturation in oxidation current was noticed after deposition for 150 s. Therefore, an NPC film prepared at −3 V for 150 s is the best choice for preparing a sensitive platform for Glyp detection.

2.2.3. pH Optimization

pH optimization is an important study for the Glyp sensor development taking into account the compound has four different pK_a values, which correspond to protonation of amino (pK_a 10.6), phosphonate (pK_a 2 and 5.6), and carboxylate (pK_a 2.6) functionalities.[50] Accordingly, the electrochemical behavior of the NPC modified Cu microelectrode at different pH values was investigated by CV in a potential window from −0.5 to 0.5 V at a 25 mV s^{-1} scan rate in PBS containing 65 nmol L^{-1} Glyp. CVs recorded in PBS of different pH values are depicted in Figure 7a, and a strong dependence of the anodic and cathodic peaks on pH is noticed. The reduction peak is sharper for CVs recorded at pH close to neutral medium (pH = 6.0, 7.0 and 8.0), which is a characteristic of faster electron transfer process associated with copper regeneration, while relatively broader peaks appear in acidic and basic conditions owing to a slower redox process involving the reduction of the copper oxide layer. The dependence of the reduction current and peak potential values on pH is shown in Figure 7b and it is clear from this plot that PBS at pH 7.0 is the best electrolytic medium to get the highest reduction current and the less negative overpotential. At pH < 4.0, Glyp becomes partially protonated, which prevents the complexation behavior, while at pH > 10.0, the decrease in the permeability of the amorphous layer of copper oxides restrains the transport of copper ions from the electrode/solution interface.[51]

2.3. Analytical Performance of the NPC-Modified Cu Microelectrode for Glyp Detection

Based on the optimized electrodeposition parameters and pH, an electroanalytical platform based on NPC for Glyp determination was developed, and different analytical parameters were assessed. The sensor performance was investigated in a 0.03 to 13 μmol L^{-1} Glyp concentration range, and for higher concentrations the calibration plot is not linear (Figure S2). Similar behavior has also been noticed by Cao et al.[27] and could be explained by the limiting amount of Cu(II) generated over the electrode surface. However, such linearity can be observed for very low Glyp concentrations. For instance, CVs of the NPC modified Cu microelectrode (E_d = −3 V and t_d = 150 s) in 0.1 mol L^{-1} PBS buffer of pH 7.0 with increasing concentration of Glyp from 30 to 65 nmol L^{-1} at a scan rate of 25 mV s^{-1} are shown in Figure 8a. As expected, an enhancement in the oxidation current and a decrease in the reduction current are observed with each successive addition of Glyp. The zoomed image in the inset of Figure 8a depicts with more details such cathodic current decrease, which is proportional to the concentration of Glyp (Figure 8b).

The calibration plot depicting the cathodic current decrease as a function of the Glyp concentration exhibits a linear correlation described by ΔI (nA) = 14 × C_{Glyp} (nmol L^{-1}) − 122 (nA) with a correlation coefficient of 0.998, where ΔI is the cathodic current difference in the absence and presence of Glyp. The slope of the correlation equation defines the sensitivity of the sensor, which was estimated as 14 nA L $nmol^{-1}$. Such a high sensitivity was expected, as it was possible to measure the signal experimentally for a 30 nmol L^{-1} Glyp, a concentration that is below the requirements of US-EPA guidelines, thus highlighting the suitability of the sensor to monitor Glyp in real samples. The limit of detection of the sensor was calculated considering the signal to noise ratio as 3, which comes out to be 3 nmol L^{-1} or 0.51 μg L^{-1}, and such very low value further strengthens our claim of the high sensitivity of the proposed NPC modified Cu microelectrode for Glyp determination.

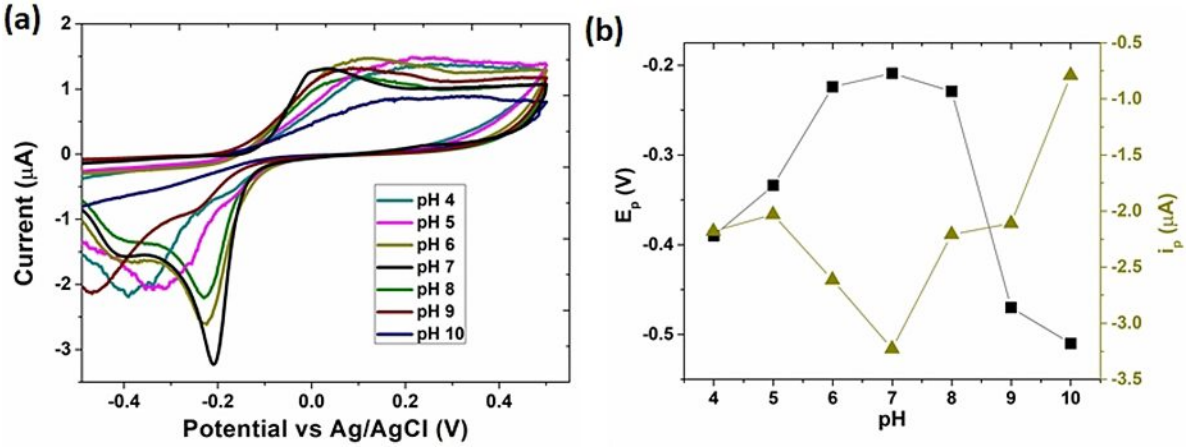

Figure 7. a) Voltammograms recorded with the NPC modified Cu microelectrode (E_d = −3 V and t_d = 150 s) in 0.1 mol L^{-1} PBS containing 60 nmol L^{-1} Glyp at different pH values. Scan rate: 25 mV s^{-1}. b) Plot of peak current (Δ) and peak potential (■) values as a function of pH.

© 2020 Wiley-VCH Verlag GmbH & Co. KGaA, Weinheim

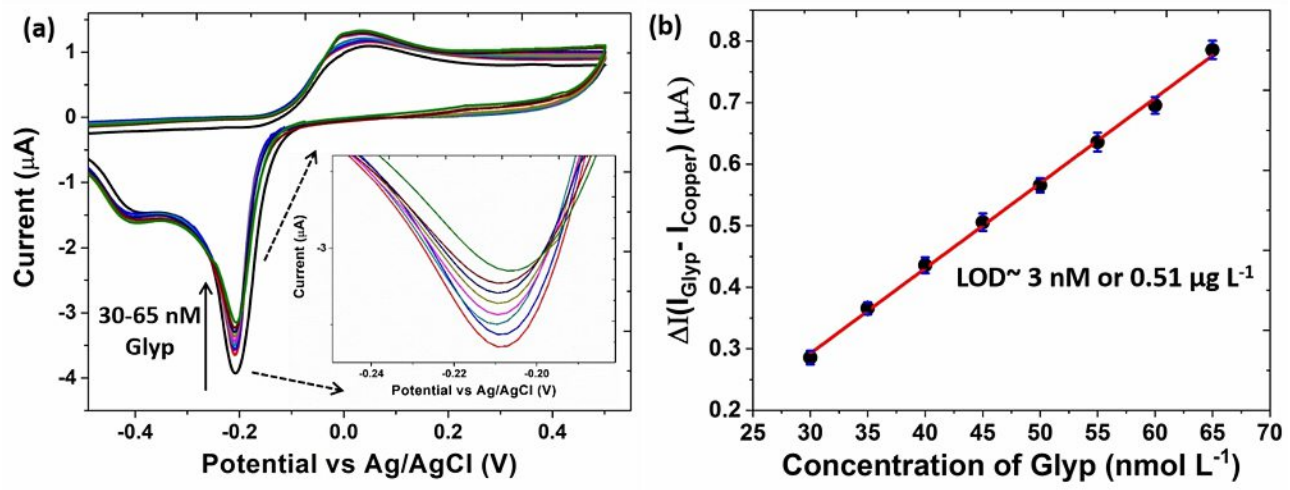

Figure 8. a) Voltammograms recorded with an NPC modified Cu microelectrode ($E_d = -3$ V; $t_d = 150$ s) in 0.1 mol L^{-1} PBS at pH 7.0 for different Glyp concentrations in the range 30 to 65 nmol L^{-1}. Scan rate: 25 mV s^{-1}. The inset presented in (a) corresponds to the magnified image of the cathodic peaks. b) Calibration plot corresponding to values of cathodic current decrease as a function of the Glyp concentration.

The selectivity of the response of the developed sensor was evaluated by recording voltammograms of Glyp in the presence of possible interfering species in concentration 10-fold higher than that of the analyte. The interferant species chosen for this study were those usually found in river waters together with Glyp. Two kinds of interferants were analyzed: in one group, other herbicides such as simazine, propazine, and atrazine, which are commonly used with Glyp in the agriculture field, and AMPA, which is the primary metabolite of Glyp. The other group included cations (Na^+, K^+, Ni^{2+}, Ca^{2+}, Mg^{2+}), which are normally present in water samples, can be coordinated by Glyp and interfere in the measurements. The influence of the possible interferents on the cathodic peak current corresponding to Glyp can be analyzed in the bar plot shown in Figure 9a. The presence of simazine, propazine, and atrazine exhibited no significant interference (less than 2%), whereas the presence of AMPA caused a more pronounced effect (at around 7%). In the case of the cations, only Ni^{2+} showed an increase in the cathodic peak current, which can be attributed to the competitive complexation of Glyp with Ni^{2+}.[52] Hence, less Glyp is available to form a complex with copper cations. Nonetheless, the influence of these interferences presents in solution at a much higher concentration than that of Glyp is not very important and can be disregarded.

The reproducibility of the sensor response was evaluated by preparing 5 different NPC modified Cu microelectrodes at identical electrodeposition conditions ($E_d = -3$ V and $t_d = 150$ s), followed by the recording of their CVs to varying concentrations

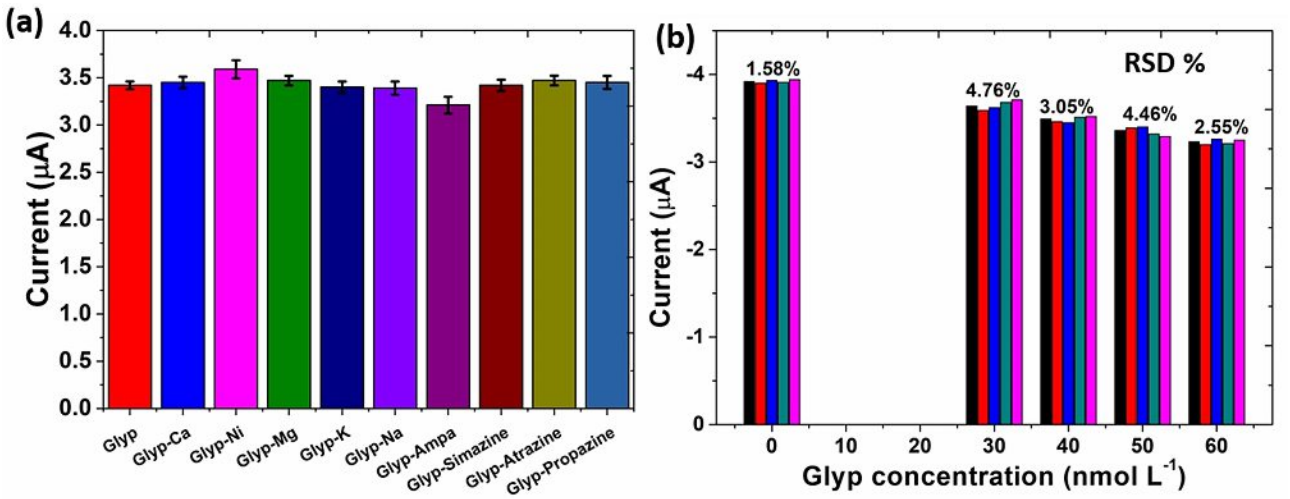

Figure 9. a) Cathodic peak current values measured with the NPC modified Cu microelectrode ($E_d = -3$ V and $t_d = 150$ s) in 0.1 mol L^{-1} PBS (pH 7.0) containing 45 nmol L^{-1} Glyp in the absence and presence of different interfering compounds (450 nmol L^{-1}). b) Cathodic peak current values measured with 5 different NPC modified Cu microelectrodes ($E_d = -3$ V and $t_d = 150$ s) in 0.1 mol L^{-1} PBS (pH 7.0) at different Glyp concentrations. Standard deviation values of the measurements are shown above the bars.

© 2020 Wiley-VCH Verlag GmbH & Co. KGaA, Weinheim

of Glyp. The reduction peak current obtained with these different NPC modified Cu microelectrodes is plotted in Figure 9b and the relative standard deviation (RSD) was less than 5% for all the studied Glyp concentrations, which confirms the high reproducibility in the preparation of the sensor.

The applicability of the proposed method was confirmed by a spike-and-recovery experiment, where known amounts of Glyp were added to river water samples, and the recovery percentage was calculated. Results of % recovery, shown in Table 1, indicate that the proposed method exhibits good accuracy and shows no interference from the sample matrix.

The analytical performance of the NPC modified Cu microelectrode for Glyp detection was finally compared with previously reported similar works, as shown in Table 2. It can be noticed that different analytical parameters like LOD and linear range of the present NPC sensor were comparable to those of other sensors.

3. Conclusions

In the present work, a highly porous and high surface area NPC film was electro-synthesized by the DHBT method, and an electroanalytical platform based on it was successfully implemented for highly sensitive and selective detection of Glyp. A thorough optimization study of electrodeposition parameters (E_d and t_d) was performed, which revealed that NPC films fabricated at $E_d = -3$ V and $t_d = 150$ s were the best sensing layer in terms of the magnitude of the measured signal. The electrodeposition produced highly pure NPC films, which was also confirmed by EDS elemental characterization. XRD measurements further revealed the presence of a highly crystalline FCC lattice of copper in (111), (220), and (200) crystallographic orientations. The morphology of the NPC films corresponds to a highly porous film containing variable-sized dendrites, which show a strong correlation with the electrodeposition conditions E_d and t_d. The fractal becomes smaller at more negative E_d and porosity increases in films prepared with more extended t_d. Such variations in the NPC morphology exert a strong influence on the electrochemical behavior of the NPC modified Cu microelectrode because more copper ions are available to diffuse through the oxide layers and interact with Glyp. Therefore, an increase in sensitivity is expected. The optimized NPC modified Cu microelectrode was tested for voltammetric determination of Glyp, and very high sensitivity (14 nA L^{-1} nmol) was achieved, with a detection limit down to 4 nmol L^{-1}. The fabricated sensor was found to be highly selective towards Glyp in the presence of common interferants. Finally, the accuracy of the NPC modified Cu microelectrode for the quantification of Glyp in river water samples was demonstrated by spike-and-recovery experiments. Hence, the electrochemical sensor developed in this study is highly promising for a simple, rapid, and cost-effective monitoring of Glyp in different environmental samples.

Table 1. Spike-and-recovery study of Glyp in spiked river water samples (95% confidence interval; n = 5).

Base[a]	Glyp added[a]	Glyp found[a]	Recovery[b] [%]
30	0	30.5 ± 0.5	-
30	5	35.2 ± 0.6	104.8
30	10	39.9 ± 0.8	98.7
30	15	45.6 ± 0.6	104.2
30	20	51 ± 1	105.2

[a] (nmol L^{-1}). [b] [(found-base)/added] × 100.

Acknowledgements

The authors would like to thank the São Paulo State Research Foundation (FAPESP 2018/08782-1, FAPESP 2019/06293-6, FAPESP 2016-07461-1, FAPESP 2019/14418-3, FAPESP 2018/16896-7) and National Council for Scientific and Technological Development (CNPq 401581/2016-0, CNP 311847-2018-8 and CNPq 402281/2013-6) for the generous funding. The authors would like to thank Prof. Koiti Araki for allowing the use of XRD facilities in his laboratory, and the Institute of Chemistry, USP, for providing SEM facilities.

Table 2. Comparison between electrochemical sensors for glyphosate determination.

Modification	Electrode	Technique	LOD [μg/L]	Linear range [μmol L^{-1}]	Reference
Copper phthalocyanine/MWCNTs[a]	GCE[b]	DPV[c]	2.02	0.83–9.9	[24]
Ni–Al LDH[d]	Platinum	Amperometry	169	10–900	[25]
Cu ion	GCE	CV	NA	5–50	[26]
Cu-BTC MOF[e]	ITO	DPV	0.24	0.001–0.09	[27]
Porous copper nanowires	Gold	Amperometry	1.69	0.01–5	[28]
TMB/HRP[f]	SPE (C)[g]	Immunoassay/Amperometry	5	0.0002–0.032	[29]
Double-template imprinted polymer-modified GNPs[h]	Carbon	DPASV[i]	0.35	0.024–1.041 & 0.0032–0.024	[30]
Nanoporous Copper	Cu μE	CV	0.51	0.030–0.065	This work

[a] Multiwall carbon nanotubes. [b] Glassy carbon electrodes. [c] Differential pulse voltammetry. [d] Nickel-aluminum layered double hydroxide. [e] Copper BTC metal-organic framework. [f] 3,3′5,5′-Tetramethylbenzidine/horseradish peroxidase. [g] Screen printed electrode (carbon). [h] Gold nanoparticles. [i] Differential pulse anodic stripping voltammetry.

© 2020 Wiley-VCH Verlag GmbH & Co. KGaA, Weinheim

Conflict of Interest

The authors declare no conflict of interest.

Keywords: electrochemical sensor · copper microelectrode · nanoporous copper · glyphosate · environmental samples

[1] H. C. Steinrücken, N. Amrhein, *Biochem. Biophys. Res. Commun.* **1980**, *94*, 1207–12.
[2] R. J. Kremer, N. E. Means, *Eur. J. Agron.* **2009**, *31*, 153–61.
[3] S. H. Bai, S. M. Ogbourne, *Environ. Sci. Pollut. Res. Int.* **2016**, *23*, 18988–9001.
[4] A. H. C. Van Bruggen, M. M. He, K. Shin, V. Mai, K. C. Jeong, M. R. Finckh, J. G. Morris, *Sci. Total Environ.* **2018**, *616–617*, 255–68.
[5] S. Braz-Mota, H. Sadauskas-Henrique, R. M. Duarte, A. L. Val, V. M. F. Almeida-Val, *Chemosphere* **2015**, *135*, 53–60.
[6] D. L. Kathryn, Z. Guyton, Y. Grosse, F. El Ghissassi, L. Benbrahim-Tallaa, N. Guha, C. Scoccianti, H. Mattock, K. Straif, *Lancet Oncol.* **2015**, *16*, 490–91.
[7] J. George, S. Prasad, Z. Mahmood, Y. Shukla, *J. Proteomics* **2010**, *73*, 951–64.
[8] S. Thongprakaisang, A. Thiantanawat, N. Rangkadilok, T. Suriyo, J. Satayavivad, *Food Chem. Toxicol.* **2013**, *59* 129–36.
[9] USEPA, (2000b) CFR, 40(2000) 136–49.
[10] E.C.D. 98/83/EEC, OJ L 330 12.05, (1998) 0032–54.
[11] C. D. Stalikas, C. N. Konidari, *J. Chromatogr. A* **2001**, *907*, 1–19.
[12] A. L. Valle, F. C. C. Mello, R. P. Alves-Balvedi, L. P. Rodrigues, L. R. Goulart, *Environ. Chem. Lett.* **2019**, *17*, 291–317.
[13] W. C. Koskinen, L. J. Marek, K. E. Hall, *Pest Manage. Sci.* **2016**, *72*, 423–32.
[14] A. Royer, S. Beguin, J. C. Tabet, S. Hulot, M. A. Reding, P. Y. Communal, *Anal. Chem.* **2000**, *72* 3826–32.
[15] Y. Zhu, F. Zhang, C. Tong, W. Liu, *J. Chromatogr. A* **1999**, *850*, 297–301.
[16] K. Sato, J.-Y. Jin, T. Takeuchi, T. Miwa, K. Suenami, Y. Takekoshi, S. Kanno, *J. Chromatogr. A* **2001**, *919*, 313–20.
[17] Z. H. Kudzin, D. K. Gralak, J. Drabowicz, J. Łuczak, *J. Chromatogr. A* **2002**, *94*, 129–41.
[18] D. Wang, B. Lin, Y. Cao, M. Guo, Y. Yu, *J. Agric. Food Chem.* **2016** *64*, 6042–50.
[19] R. Muñoz, A. Guevara-Lara, J. L. M. Santos, J. M. Miranda, J. A. Rodriguez, *Microchem. J.* **2019**, *146*, 582–87.
[20] S. J. Noori, M. Dimaki, J. Mortensen, E. W. Svendsen, *Sensors* **2018**, *18(9)*, 2961–70.
[21] R. Bataller, I. Campos, N. Laguarda-Miro, M. Alcañiz, J. Soto, R. Martínez-Máñez, L. Gil, E. G. Breijo, J. Civera, *Sensors* **2012**, *12*, 17553–68.
[22] E. V. Sierra, V. M. Sarria, M. T. Cortés, *Quim. Nova* **2008**, *31*, 220–26.
[23] C. F. B. Coutinho, L. F. M. Coutinho, L. H. Mazo, S. L. Nixdorf, C. A. P. Camara, F. M. Lanças, *Anal. Chim. Acta* **2007**, *592* 30–35.
[24] F. C. Moraes, L. H. Mascaro, S. A. S. Machado, C. M. A. Brett, *Electroanalysis* **2010**, *22*, 1586–91.
[25] A. Khenifi, Z. Derriche, C. Forano, V. Prevot, C. Mousty, E. Scavetta, B. Ballarin, L. Guadagnini, D. Tonelli, *Anal. Chim. Acta* **2009**, *654*, 97–102.
[26] S. Pintado, M. R. Montoya, R. R. Amaro, M. Mayén, J. M. R. Mellado, *Int. J. Electrochem. Sci.* **2012**, *7*, 2523–30.
[27] Y. Cao, L. Wang, C. Shen, C. Wang, X. Hu, G. Wang, *Sens. Actuators B* **2019**, *283*, 487–94.
[28] S. Poorahong, C. Thammakhet, P. Thavarungkul, P. Kanatharana, *Chem. Pap.* **2015**, *69*, 385–94.
[29] F. Bettazzi, A. R. Natale, E. Torres, I. Palchetti, *Sensors* **2018**, *18*, 2965.
[30] B. B. Prasad, D. Jauhari, M. P. Tiwari, *Biosens. Bioelectron.* **2014** *59*, 81–88.
[31] W. B. Liu, S. C. Zhang, N. Li, J. W. Zheng, Y. L. Xing, *Microporous Mesoporous Mater.* **2011**, *138*, 1–7.
[32] N. Wang, Y. Pan, S. Wu, E. Zhang, W. Dai, *RSC Adv.* **2017**, *7*, 43255–65.
[33] H. Qiu, T. Tang, M. Asif, X. Huang, Y. Hou, *Adv. Funct. Mater.* **2019**, *29*, 1808468.
[34] M. Wang, X. Yu, Z. Wang, X. Gong, Z. Guo, L. Dai, *J. Mater. Chem. A* **2017**, *5*, 9488–513.
[35] S. Sattayasamitsathit, P. Thavarungkul, C. Thammakhet, W. Limbut, A. Numnuam, C. Buranachai, P. Karatharana, *Electroanalysis* **2009**, *21*, 2371–77.
[36] Y. Li, J. Z. Sun, C. Bian, J. H. Tong, H. P. Dong, H. Zhang, S. H. Xia, *AIP Adv.* **2015**, *5*, 041312.
[37] M. R. Majidi, S. Ghaderi, *Talanta* **2017**, *175*, 21–29.
[38] J. Yang, J. Chen, Y. Zhou, K. Wu, *Sens. Actuators B* **2011**, *153*, 78–82.
[39] B. J. Plowman, L. A. Jones, S. K. Bhargava, *Chem. Commun.* **2015**, *51*, 4331–46.
[40] A. P. R. Souza, M. O. Salles, E. S. Braga, M. Bertotti, *Electroanalysis* **2011**, *23*, 2511–15.
[41] G. A. Hope, R. Woods, *J. Electrochem. Soc.* **2004**, *151*, C550-C53.
[42] N. Sreeju, A. Rufus, D. Philip, *J. Mol. Liq.* **2016**, *221*, 1008–21.
[43] A. V. Limaye, R. E. Amritkar, *Phys. Rev. A* **1986**, *34*, 5085–90.
[44] T. A. Witten, L. M. Sander, *Phys. Rev. Lett.* **1981**, *47*, 1400–03.
[45] A. Kumar, J.M. Gonçalves, A. Sukeri, K. Araki, M. Bertotti, *Sens. Actuators B* **2018**, *263*, 237–47.
[46] C. D. Owen, M. Grant Norton, *J. Mater. Sci.* **2016**, *51*, 577–88.
[47] H. C. Shin, J. Dong, M. Liu, *Adv. Mater.* **2003**, *15*, 1610–14.
[48] P. G. Daniele, C. De Stefano, E. Prenesti, S. Sammartano, *Talanta* **1997**, *45*, 425–31.
[49] T. Undabeytia, E. Morillo, C. Maqueda, *J. Agric. Food Chem.* **2002**, *50*, 1918–21.
[50] C. M. E. Morillo, M. Bejarano, L. Madrid, T. Undabeytia, *Chemosphere* **1994**, *28*, 2185–96.
[51] C. F. B. Coutinho, M. O. Silva, S. A. S. Machado, L. H. Mazo, *Appl. Surf. Sci.* **2007**, *253*, 3270–75.
[52] V. Subramaniam, P. E. Hoggard, *J. Agric. Food Chem.* **1988**, *36*, 1326–9.

Manuscript received: January 13, 2020
Revised manuscript received: February 6, 2020
Accepted manuscript online: February 6, 2020

© 2020 Wiley-VCH Verlag GmbH & Co. KGaA, Weinheim